

# Journal of Materials Chemistry A

Accepted Manuscript



This is an *Accepted Manuscript*, which has been through the Royal Society of Chemistry peer review process and has been accepted for publication.

*Accepted Manuscripts* are published online shortly after acceptance, before technical editing, formatting and proof reading. Using this free service, authors can make their results available to the community, in citable form, before we publish the edited article. We will replace this *Accepted Manuscript* with the edited and formatted *Advance Article* as soon as it is available.

You can find more information about *Accepted Manuscripts* in the [Information for Authors](#).

Please note that technical editing may introduce minor changes to the text and/or graphics, which may alter content. The journal's standard [Terms & Conditions](#) and the [Ethical guidelines](#) still apply. In no event shall the Royal Society of Chemistry be held responsible for any errors or omissions in this *Accepted Manuscript* or any consequences arising from the use of any information it contains.

## ARTICLE

# Conductive Cellulose Nanocrystals with High Cycling Stability for Supercapacitor Applications

Cite this: DOI: 10.1039/x0xx00000x

Xinyun Wu<sup>1</sup>, Juntao Tang<sup>1</sup>, Yuchen Duan<sup>1</sup>, Aiping Yu<sup>1</sup>, Richard M Berry<sup>2</sup>, Kam C Tam<sup>1,\*</sup>Received 00th January 2012,  
Accepted 00th January 2012

DOI: 10.1039/x0xx00000x

www.rsc.org/

A facile method of polymerizing polypyrrole (PPy) on poly(N-vinylpyrrolidone) (PVP) coated cellulose nanocrystals (CNCs) was developed. The PPy/PVP/CNCs possessed a well-defined core-shell structure with well-preserved one-dimensional (1D) fibril geometry. Stable hybrid CNC was produced and no PPy particles were formed in the bulk solution. Significant improvement in the electrochemical performance was achieved when compared to PPy coated Tempo-CNC reported previously. A high conductivity of 36.9 S/cm was achieved with an excellent specific capacitance of 322.6 F/g and improved cycling stability of less than 9 and 13% loss after 1000 and 2000 cycles respectively. The strategy of using PVP as an effective surface modifier to improve the conductive polymer deposition on CNC proves to be a critical necessary step.

## 1. Introduction

The increasing demand for various consumer electronics and hybrid vehicles capable of delivering a high power in short pulses with an extremely long cycle life has prompted renewed interest in supercapacitors (SPs). Polypyrrole (PPy) has been extensively studied for decades as a promising electrode material for SPs due to its ease of synthesis, low cost, good conductivity, stability<sup>1,2</sup> and excellent specific capacitance (Cs).<sup>3</sup> However, being mechanically weak, PPy experiences significant structural breakdown resulting from volumetric swelling/shrinkage resulting in a fast capacitance decay over extended cycles (less than 50% retention of the initial capacitance after 1000 cycles).<sup>4,5,6</sup> Another drawback is the poor processibility and unsatisfactory specific capacitance (Cs) (F/g) due to agglomeration resulting from strong intermolecular, intramolecular interactions and possible cross-linking of PPy chains.<sup>7,8</sup>

The key to addressing these shortcomings will depend on the controlled synthesis of the active material. Generally, a large surface area between electrode material and electrolyte is critical for improving the capacitance, because of enhanced ion mobility. A thin and uniform coating of active material is also necessary for a fast and effective ion diffusion in the polymer matrix. With the advent of nanotechnology, various polypyrrole-based nanocomposites were developed by polymerizing polypyrrole as a thin layer on another template material, such as graphite<sup>9</sup>, carbon nanotubes (CNT)<sup>10-15</sup>, graphene oxides (GO)<sup>10,16-19</sup>. Large increase in the surface area arising from the nanosize effect of these PPy-based hybrid nanocomposites produced higher Cs compared to their bulk counterparts. Improved cycling stability was also achieved due to the enhanced reinforcement, e.g. PPy/GO achieved 249 F/g of Cs with 81% of the Cs retention after 1000 cycles under 0.3 A/g.<sup>20</sup> A Cs of 183.2 F/g at a high current density of 8 A g<sup>-1</sup>

was obtained for CNT embedded PPy network with Cs retention of 85% after 1000 cycles at 1 A/g.<sup>21</sup>

Recently, several research efforts have been devoted to PPy/cellulose nanocomposites, due to their abundance, lightweight, good mechanical property, abundant hydroxyl group for further functionalization, biodegradability and low cost. Many PPy/nanocellulose hybrids were synthesized via chemical polymerization in the form of films, gels, or cakes, due to the length of entangled cellulose network.<sup>22-27</sup> More recently, individually coated nanocellulose was achieved on cellulose nanocrystals (CNCs)<sup>28-30</sup>. These rice-shaped nanoparticles (100-400 nm long, 5-20 nm in diameter) are extracted from cellulose fibres by removing the amorphous region via acid hydrolysis yielding well-dispersed nanoparticles with high density of surface sulfuric acid groups. Liew *et al.* reported the successful synthesis of PPy/CNC via electrochemical deposition and demonstrated that the capacitance was comparable to PPy/CNTs synthesized under similar conditions. The high capacitance is largely attributed to the highly porous structure, thin coating of PPy on individual fibers, and rigidity of CNC substrate.<sup>28,29</sup> However, the end product from electrodeposition is a dense film on the electrode that limits further processing. Using a facile in situ chemical polymerization, our recent study on a PPy/CNC system with a core-shell structure possessed attractive supercapacitor behavior.<sup>30</sup>

Despite the success in the development of PPy-coated nanocomposites, the precise control of a uniform and thin PPy morphology at nanoscale remained a significant scientific challenge, hindering the commercial application of these composite electrode material. It is difficult to fully prevent the formation of free PPy particles in bulk solution, and deposited conjugated polymers on the nanoparticles are often irregular and thick. In most cases, the PPy-based hybrid material loses

its fine fibril structure due to agglomerations.<sup>31</sup> Our previous strategy to improve the affinity between CNC and PPy coating via additional hydrogen bonding sites did not completely eliminate the formation of PPy particles and the irregular PPy coatings.<sup>30</sup> Previous studies have found that conductive polymers such as PPy favor the growth on CH<sub>3</sub> terminated hydrophobic regions than hydrophilic OH groups.<sup>32</sup> Several studies have demonstrated that the deposition of PPy onto relatively hydrophobic polystyrene latex particles<sup>33,34</sup> led to a much smoother, and continuous coating, while the deposition onto more hydrophilic poly(methyl methacrylate) latex produced discontinuous and patchy PPy coating.<sup>35,36</sup> Studies on PPy coated micro-sized silica particles with hydrophilic silanol groups led to highly globular-surfaced particles that aggregated to form 'raspberry'-like structure.<sup>37</sup> This problem can be addressed through a simple pretreatment with either silanes via chemical grafting, or coating of a monolayer of poly(N-vinylpyrrolidone)(PVP), to yield a uniform PPy coating on the substrate.<sup>38,39,40,41</sup>

In this paper, we report on the development of a core-shell PPy/PVP/CNC nanorod that displays a smooth and uniform PPy coating. Surface modification on CNC was achieved through the physical adsorption of PVP to alter the hydrophilic nature of CNC for the favorable growth of PPy. PVP also acts as a steric stabilizer to prevent PPy-coated hybrid particles from further agglomeration. The degree of surface modification of CNC was also systematically evaluated since it is a crucial parameter to achieve an optimal PPy deposition. The optimally synthesized PPy/PVP/CNC on an insulating template possesses superior conductivity and demonstrates improved capacitance and cycling stability for SP applications. The current synthesis and characterizations were compared to the PPy/Tempo CNC system reported recently by our group.

## 2. Experimental Section

### 2.1 Materials

Cellulose nanocrystal (CNC) was provided by FP Innovations and Celluforce Inc. The chemicals used in this study were reagent grade, purchased from Sigma-Aldrich, and used as received. The chemicals for reaction are: poly(N-vinylpyrrolidone) (PVP) (MW 10,000 Da), Iron(III) chloride (97%), and pyrrole (98%).

### 2.2 Synthesis of PPy/PVP/CNC hybrid nanostructure

The surface-modified CNCs were first prepared by mixing 0.2 wt% CNC solution with PVP at different PVP/CNC mass ratio of 100/0, 40/60, 10/90, 5/95, and 0/100 (samples denoted as PVP100/CNC, PVP 40/CNC, PVP10/CNC, PVP5/CNC and PVP0/CNC respectively). The dispersion was mixed for 24 hours to ensure sufficient adsorption of PVP on CNC surface, which is referred herein as PVP/CNC.

In one typical polymerization for PPy/PVP/CNC, 15 ml of PVP/CNC solution was transferred to a double-jacketed reaction vessel kept in an ice water bath at 0 °C. Then 364.5 mg of FeCl<sub>3</sub> dissolved in 5ml water was added dropwise to the suspension and vigorously stirred. After an hour, 106.5 μl of pyrrole monomer (Py) dissolved in 5 ml water was added slowly and the polymerization was left to mix under mild stirring for 16 hours, and the reaction was quenched by repeated washing with DI water in an ultrafiltration cell. Finally, the precipitates were freeze-dried, and the dried fine powder and was pressed into pellet for conductivity measurements.

### 2.3 Characterization

The morphology of PPy/PVP/CNC system was characterized using a Philips CM10 electron microscope. Transmission electron microscope (TEM) samples were prepared by depositing one drop of 0.01wt% sample onto a carbon coated copper grid and dried at room temperature. The same TEM sample grid was used directly for Scanning electron microscopy (SEM) imaging (Philips XL-30 microscope) and by attaching onto carbon tape. The zeta potential of the PPy/CNC system was monitored throughout the polymerization process using a Malvern Zetasizer Nano ZS (Worcestershire, UK). Sample aliquots were collected from the reaction vessel at different time intervals, filtered with DI water and measured. The zeta potential of the particles was calculated from the electrophoretic mobility values using the Smoluchowski equation. The thermal stability of the PPy/PVP/CNC systems were studied by thermal gravimetric analysis (TGA). All samples were placed in an inert ceramic crucible and heated from 25 to 800 °C at a heating rate of 10°C min<sup>-1</sup> in 20 mL min<sup>-1</sup> of air.

### 2.4 Electrochemical Measurements

Conductivity was measured using an in-house four-probe station. The freeze-dried bulk powder of PPy/PVP/CNC was pressed into thin rectangular pellets and the conductivity  $\alpha$  in S/cm was calculated using the expression:

$$\alpha = (D/R) \times (1/WT)$$

where D is the distance between the electrodes, R is the measured resistance of the pellet, W and T is the width and thickness of the pellet respectively.

Cyclic Voltammetry (CV) was conducted using a CHI 760D electrochemical station (CH Instruments, USA) equipped with a three-electrode half-cell configuration with a platinum electrode and a saturated calomel reference electrode (SCE). Cyclic voltammetry (CV), charge and discharge (CD), and electrochemical impedance spectroscopy (EIS) were performed following a 25-cycle CV activation between -0.6 and 0.4 V versus SCE in KCl electrolyte (0.5 M). The working electrode was fabricated by repeated casting (twice) of the PPy/CNC (1 mg mL<sup>-1</sup> in 50% water/ethanol) dispersion onto the graphite carbon (GC) electrode (3 mm in diameter) at 10 μL each time and dried (mass loading on the electrode for testing is 20 μg). The CV test was performed with scan rates of 1, 10, and 100 mV.s<sup>-1</sup>. The capacitance obtained from the CV curve was calculated as follows:

$$C_s = \frac{\int idV}{2 \times m \times \Delta V \times S}$$

where C<sub>s</sub> is the specific capacitance,  $\int idV$  is the integrated area of the CV curve, m is the mass of active material,  $\Delta V$  is the potential range, and S is the scan rate. Cycling stability test was carried out under the same experimental setup at a scan rate of 100 mV.s<sup>-1</sup>.

Charge and discharge (CD) tests were performed by applying a constant current density of between 2 to 10 A g<sup>-1</sup>. The cell capacitance was determined from the CD curve using the equation below:

$$C = I / (dV/dt)$$

where dV/dt was calculated from the slope of the CD discharge curve, and I is the charge current density (A g<sup>-1</sup>). Cycling stability was performed with the same testing setup at 10 A g<sup>-1</sup>.

### 3. Results and Discussion

The experimental strategy for the synthesis of the core-shell structured PPy/PVP/CNC is illustrated in Fig. 1. Surface modified CNC was simply achieved by mixing PVP with CNC. After PVP was physically adsorbed on the CNC surface, the oxidant and the monomer were then introduced.

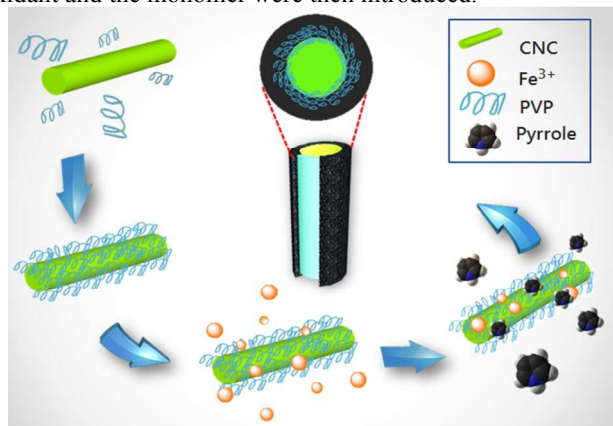


Fig. 1. Schematic illustrating the formation of proposed core-shell PPy coated CNC. PVP was adsorbed onto the CNC surface prior to the polymerization to promote the homogeneous growth of PPy shell.

The degree of CNC surface modification with PVP and its effect on PPy growth were characterized with a TEM and shown in Fig. 2. A noticeable size expansion was observed in Figs. 2(b) - (f) for all the PPy/CNCs synthesized at different PVP/CNC ratio confirming the successful polymerization of PPy shell. The fibril shape of CNCs with 150-250 nm in length was preserved after PPy coating. The most attractive feature of the PPy coating using this protocol is the continuous and uniform PPy coating. During our synthesis, we observed an appreciable increase in the polymerization kinetics from PVP100/CNC to PVP0/CNC based on the accelerating color change from light yellow to black, which was confirmed using a TEM. In Fig. 2(b), CNCs were not completely covered by PPy and the magnified image clearly showed some exposed CNC surface that was not coated with PPy. By decreasing the PVP/CNC mass ratio to 10, a more uniform PPy coating with a thicker shell was formed on the CNC. When the PVP/CNC ratio was reduced, the PPy coating became inhomogeneous (Fig. 2(e)). When no PVP was added, the PPy coatings were irregular and rougher, caused by the fast polymerization rate resulting in agglomeration (Fig. 2(f)). TGA studies (data in supplementary material Fig. S1) for PPy/PVP100/CNC and PPy/PVP10/CNC also suggested a more efficient growth of PPy layer at a lower CNC modification degree with enhanced thermal stability.

To highlight the important role of PVP in the synthesis process, we mixed equal mass of pristine CNC with PVP modified CNC, and performed the polymerization in the same reaction vessel. Interestingly, the TEM image revealed two dramatically different phenomena: polypyrrole was exclusively grown on PVP coated CNC, while those without PVP displayed inhomogeneously coated and globular PPy particles deposited on CNC surface. (Fig. 3) The PVP is believed to serve two functions: (i) firstly, being an amphiphilic polymer, PVP provides hydrophobic domain that promotes a favorable growth of PPy on CNC surface; (ii) secondly, being a macromolecule, it acts as steric stabilisers that minimizes the agglomeration of

PPy/CNC particles producing stable PPy/PVP/CNC hybrid nanoparticles in aqueous solution.<sup>39</sup> In addition, hydrogen bonding between the carbonyl groups of PVP and the N-H group of Py promotes a uniform growth of PPy on PVP-coated CNC.

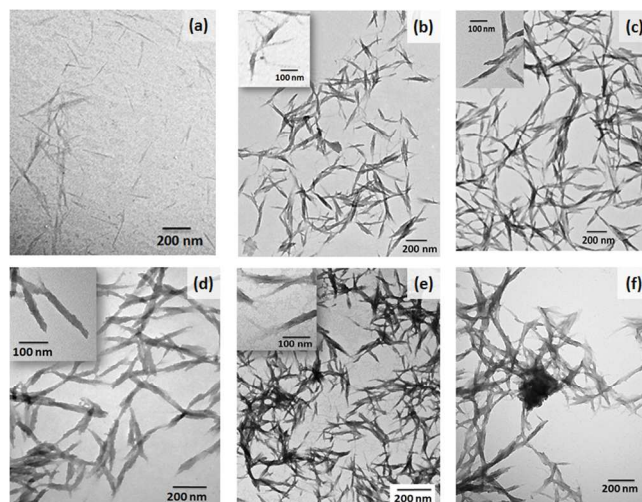


Fig. 2. TEM images for (a) pristine CNC; (b) PPy/PVP100/CNC; (c) PPy/PVP40/CNC; (d) PPy/PVP10/CNC; (e) PPy/PVP5/CNC; (f) PPy/PVP0/CNC

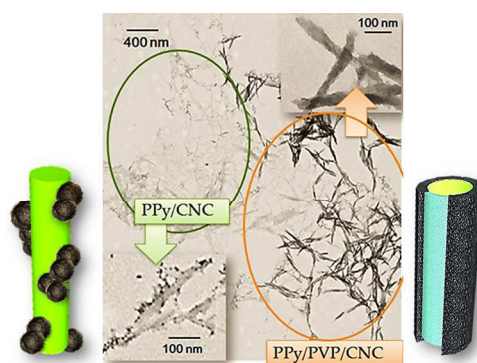


Fig. 3. PPy polymerization in the presence of equal amounts of pristine CNCs and PVP/CNCs with cartoon illustrating the two drastically different morphologies of the end products.

The conductivity of PPy/PVP/CNC samples prepared at different PVP/CNC ratio were evaluated and summarized in Fig. 4(a) together with the zeta potential (ZP). Due to the negatively charged sulfuric acid groups on the surface (i.e.  $\text{OSO}_3^-$ ), CNC possessed a negative ZP of -55 mV and is extremely stable in aqueous solution. Coating of PPy neutralized the surface negative charges on CNC by the positively charged PPy backbone. From PPy/CNC10/CNC, the ZP increased sharply to a positive value signifying a homogeneous coating of PPy on CNC (i.e. CNCs are fully covered with PPy layers, thereby shielding the sulfuric acid groups). This correlates with the conductivity data, where PPy/CNC10/CNC possessed the highest conductivity and the most positive ZP. However, when PVP addition was insufficient (less than 5% PVP), the ZP decreased to a negative value, indicating a non-uniform PPy coating on the CNC. The conclusions based on ZP measurements agreed with the TEM observations for all the samples prepared at different PVP/CNC as shown in Fig. 2(b)-

(f). The reaction kinetics of the PPy/PVP10/CNC sample were examined by monitoring the changes in ZP over a period of 24 hours, and Fig. 4(b) summarises the conductivity and zeta potential as a function of time. The ZP results suggested that the polymerization occurred rapidly in the first 3 hours, and it plateaued after 10 hrs. The PPy growth on the surface of CNC approached the conducting percolation threshold at 3 hours with the conductivity reaching a plateau and remained constant for the next 10 hrs and it decreased rapidly after 16 hours. This is not unexpected since extended polymerization often leads to overoxidation that disrupts the ordered conjugated structure of conductive polymers<sup>42</sup>. The inset TEM image shows the PPy/PVP10/CNC sample at 24 hours. Compared with the sample at 16 hours (Fig. 2(d)), the surface morphology of PPy layer at 24 hours polymerization was much rougher and fluffier, which confirmed our earlier hypothesis.

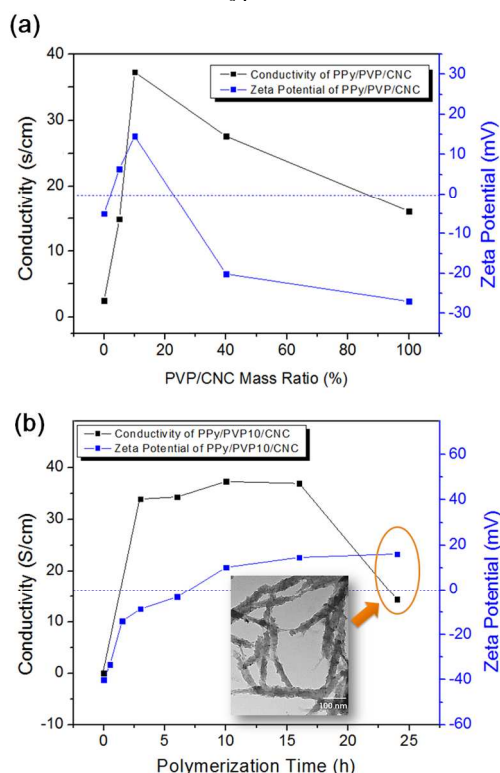


Fig.4. (a) The effect of the degree of surface modification on CNC on the zeta-potential and conductivity of the hybrid material of PPy/PVP/CNC after polymerization. (b) Kinetic study: the effect of polymerization time on the conductivity and zeta-potential of PPy/PVP10/CNC. TEM image shows the morphology of PPy/PVP10/CNC sample under polymerization time of 24 hours.

Cyclic Voltammetry (CV) was conducted on different PPy/PVP/CNC systems. The  $C_s$  result from CV tests of different PPy/PVP/CNC samples were plotted and compared in Fig. 5(a). The specific capacitance continued to increase from 3 hours until it approached a peak value of between 260 to 320 F/g at 16 hours, and it decreased sharply after that. It is interesting to compare the CV results with the conductivity data in Fig. 4(b). Though the conductivity approached a threshold at 3 hours, the capacitance did not. The capacitance reached its optimal levels when CNC/PVP was evenly coated with PPy.

The sharp decrease in the capacitance was attributed to the thick and rougher PPy coating, which hindered the ion diffusion and charge transfer. The best performance of PPy/PVP10/CNC in the CV test possessed a capacitance of 323 F/g, which holds promise for supercapacitor application. The superior  $C_s$  is mainly due to the nanoporous network formed by the 1D rod-shaped PPy/PVP/CNCs that possessed significant active surface area for the efficient ion diffusion and transport (the FESEM image of the deposited PPy/PVP/CNC film on the working electrode shown in the bottom of Fig. 5(a)). Moreover, the lightweight substrate material of CNC and ultrathin and uniform layer of PPy coating also contribute to the high  $C_s$ .

To further investigate electrochemical performances of the PPy/PVP/CNC nanocomposite system, galvanostatic charge-discharge (CD) process was performed on the optimal PPy/PVP10/CNC sample at various current densities. The CD curves possessed a triangular symmetry and linear slopes, confirming its good electrochemical performance. When lower current density was applied, the discharge curve displayed a slight curvature, representing the pseudocapacitive behavior. The calculated capacitance approached  $338.6 \text{ F g}^{-1}$  at  $2 \text{ A g}^{-1}$ . It is also worth noting that the PPy/PVP/CNC electrode displayed only a moderate drop, i.e. 5.4% of the  $C_s$ , when the current density was increased from 2 to  $10 \text{ A g}^{-1}$ . This indicates that the utilization efficiency of the active material of PPy coating was maintained at a high level at high charge current. Moreover, the IR drop in CD curves due to internal resistance of the electrode material was not observed in the PPy/PVP/CNC system.

The stability during charge and discharge is a critical issue that is closely associated with the properties/morphologies of the active material. Fig. 5(c) shows the cycling stability of the as-prepared PPy/PVP10/CNC nanostructures by conducting CD tests at a current density of  $10 \text{ A g}^{-1}$ . The  $C_s$  retained 87.3% of its initial value over 2000 cycles, confirming the excellent stability of the system. Moreover, the sharpest drop in  $C_s$  occurred in the first 400 cycles, presumably due to the loss of active material that was loosely attached on the carbon electrode. The reduction in  $C_s$  became less significant between 400 to 2000 cycles, which implies a good mechanical stability and capacitive behaviour of PPy/PVP/CNC.

We compared the current synthesis with our previous system prepared using TEMPO-oxidized CNCs (Tab. 1).<sup>30</sup> The key advantages of the new approach are: (i) the synthesis is conducted in mild pH condition, instead of extremely low pH environment needed for TEMPO-CNC; (ii) physical adsorption of PVP onto CNC is much simpler than TEMPO-mediated oxidation of CNC for enhanced affinity between the substrate and PPy.

The important properties of PPy coated CNC using two different approaches are summarized and compared in Table 1. Firstly, the ZP of PPy/PVP10/CNC was positive while PPy/Tempo-CNC possessed a negative ZP at -31mV, suggesting that a more uniform and better coating of PPy was achieved for PVP/CNC system. Secondly, the conductivity of PPy/PVP/CNC increased 7 fold (conductivity increased from 4.9 to 36.9 S/cm), which is largely attributed to the improved PPy coating as confirmed by TEM images of both samples (Fig. 5(b) and (c)). PPy/Tempo-CNC produced a globular PPy coating morphology with sporadic coverage on the CNC nanorods, whereas PPy/PVP/CNC displayed a uniform core-sheath structure covering most of the CNC surface. An enhancement of 35% in the specific capacitance was observed for the PPy/PVP/CNC system.

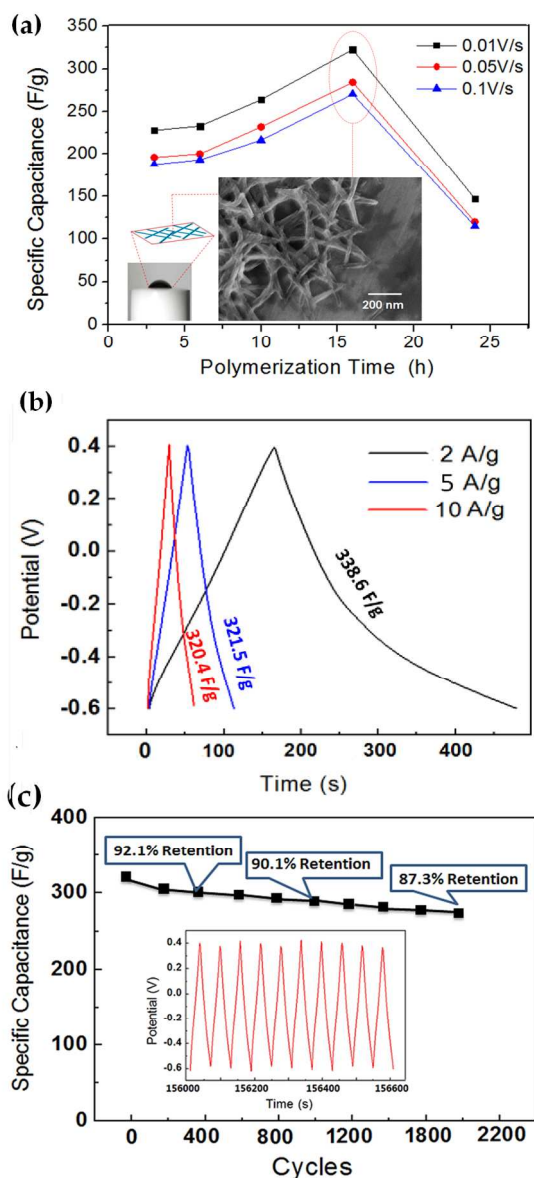


Fig. 5 (a) Specific capacitance from CV test for PPy/PVP10/CNC polymerized at different time intervals. The FESEM image shows the porous structure formed by drop casting PPy/PVP10/CNC solution on the working electrode. (b) charge-discharge curves of PPy/PVP10/CNC electrode at different current densities. (c) Cycling performance of the PPy/PVP10/CNC electrode at the current density of  $10 \text{ A g}^{-1}$ . The inset shows the charge-discharge curves of the last 10 cycles.

The same CV stability tests were also performed on PPy/Tempo-CNC (Py/OH=16) and PPy/PVP16/CNC. The CV curves at different cycling numbers are shown in Fig. 6(a) and 6(b), and the capacitance loss over cycling was plotted in Fig. 6(c). The cycling stability was greatly enhanced in the PPy/PVP/CNC system with less than a 9% capacitance loss compared to a 35% loss for the PPy/Tempo-CNC system. The superior cycling stability is attributed to a more uniform PPy deposition that facilitates the charge transfer and diffusion. In addition, the affinity between PVP and PPy driven by hydrophobic interaction and hydrogen bonding provided a

stronger and robust PPy coating. The enhanced cycling stability could also be due to the pseudo-3-layer structure of the PPy/PVP/CNC. The layer in the middle formed by PVP polymer chains serves as a buffer that effectively releases stress induced by ion diffusion/electron transfer within the hybrid material (illustrated in Fig. 6(d)). This is especially advantageous compared to the 2-layered PPy/CNC model where there is no binder at the interface to provide flexibility between the substrate and the PPy sheath.

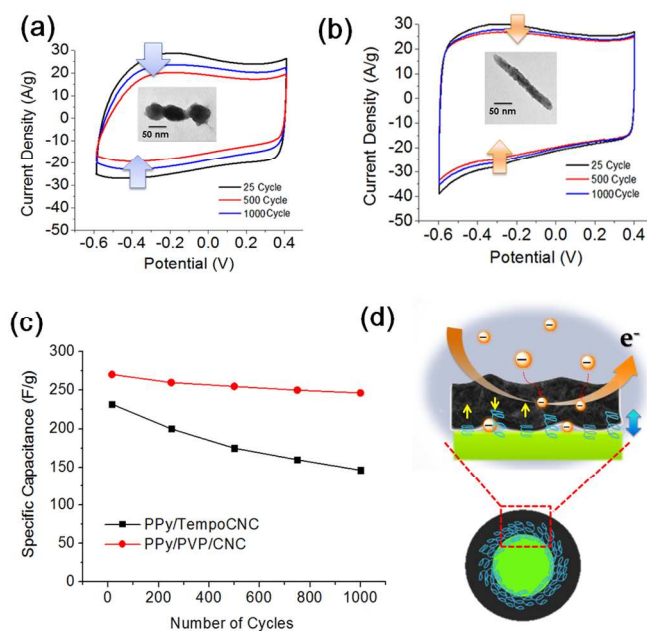


Figure 6(a) CV curve of different cycles for sample PPy/TempoCNC during 1000 cycles at 0.1 V/s scan rate. The TEM image shows the typical morphology of PPy/TempoCNC. (b) CV curve of different cycles for sample PPy/PVP/CNC during 1000 cycles at 0.1 V/s scan rate. The TEM image shows the typical morphology of PPy/PVP/CNC. (c) Comparison of Capacitance loss between PPy/PVP10/CNC and PPy/Tempo-CNC (d) Proposed mechanism that PVP layer as a binder releases the stress and provides better accommodation for the conformational change for PPy during cycling.

		PPy/TempoCNC	PPy/PVP/CNC
Synthesis	PH	Low	Neutral
	Surface modification of CNC	TEMPO-mediated Oxidation	PVP adsorption
Zeta Potential		- 31mV	+ 16.1 mV
Conductivity		4.9 S/cm	36.9 S/cm
Specific Capacitance	0.01 V/s	238.8 F/g	322.6 F/g
	0.05 V/s	224.7 F/g	284.2 F/g
	0.1 V/s	219.8 F/g	270.4 F/g
Capacitance Loss after 1000 cycles		36.9%	8.9%

Tab. 1. Comparison in synthesis and key characterizations of the improved PPy/PVP/CNC and PPy/TempoCNC system.

#### 4. Conclusion

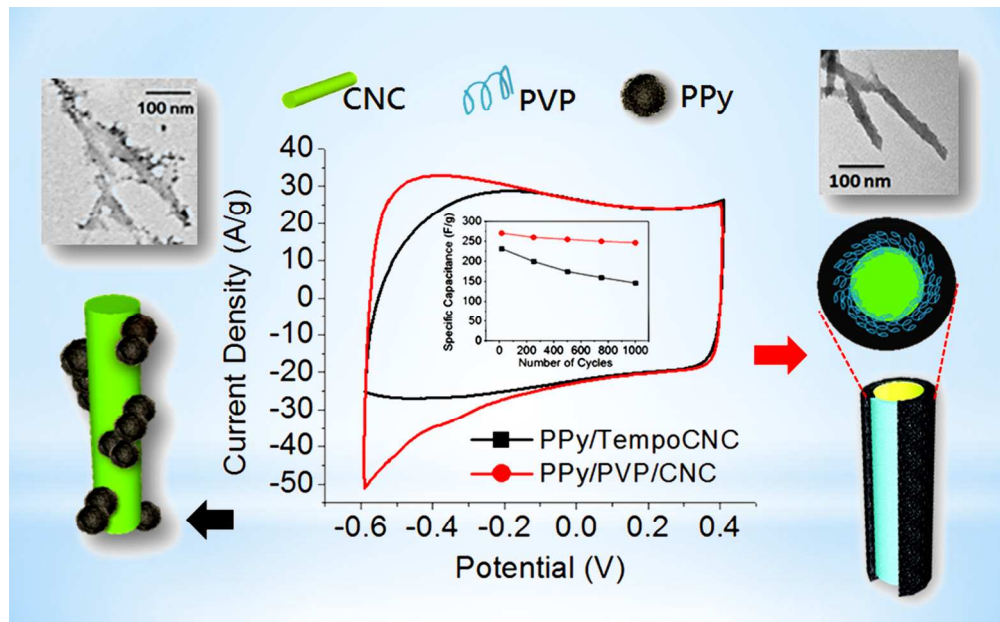
We reported on the synthesis of a core-shell PPy/CNC hybrid nanostructure with uniform and smooth PPy coating deposited on the pretreated PVP/CNC surface. The physical adsorption of PVP onto CNC surface prior to the introduction of pyrrole plays a critical role in ensuring a uniform polypyrrole coating. PVP introduces hydrophobicity to CNC surface making it much more favorable for the growth of the hydrophobic PPy shell that acts as steric stabiliser preventing further agglomeration of the nanoparticles. An outstanding conductivity of 36.9 S/cm was achieved for the PPy/PVP/CNC synthesized with 10% PVP to CNC mass ratio. The calculated capacitance approaches  $338.6 \text{ F g}^{-1}$  at  $2 \text{ A g}^{-1}$  with a good Cs retention of 87.3% over 2000 cycles. The same CV measurement was performed and compared with our previous traditional chemical synthesis conducted over PPy coated Tempo-CNC system. An enhancement of 35% in the specific capacitance was observed for the PPy/PVP/CNC system with much improved cycling stability (less than 9% Cs loss over 1000 cycles) at 0.1 V/s fast scan rate. The current system displayed a more efficient and uniform growth of PPy coating with improved electrochemical behaviors (conductivity, Cs, Cycling stability). We believe the proposed approach of surface functionalization with PVP offers an attractive approach to produce conductive hybrid composite system with enhanced electrochemical performance.

#### Acknowledgments

We wish to acknowledge FP Innovations for providing the cellulose nanocrystals. The research funding from CelluForce and AboraNano facilitated the research on conductive CNC. K. C. Tam wishes to acknowledge fundings from CFI and NSERC.

#### References

- K. S. Ryu, K. M. Kim, N. G. Park, Y. J. Park, and S. H. Chang, *J. Power Sources*, 2002, 103, 305–309.
- A. Rudge, I. Raistrick, S. Gottesfeld, and J.P. Ferraris, *Electrochim. Acta*, 1994, 39, 273–287.
- G. A. Snook, P. Kao, and A. S. Best, *J. Power Sources*, 2011, 196, 1–12.
- G. Wang, L. Zhang, and J. Zhang, *Chem. Soc. Rev.*, 2012, 41, 797–828.
- T. Liu, L. Finn, M. Yu, H. Wang, T. Zhai, X. Lu, Y. Tong, and Y. Li, *Nano Lett.*, 2014, 14, 2522–2527.
- Y. Zhao, B. Liu, L. Pan, and G. Yu, *Energy Environ. Sci.*, 2013, 6, 2856–2870.
- L. Z. Fan and J. Maier, *Electrochem. commun.*, 2006, 8, 937–940.
- F.-H. Hsu and T.-M. Wu, *Synth. Met.*, 2012, 162, 682–687.
- J. H. Park, J. M. Ko, O. O. Park, and D.-W. Kim, *J. Power Sources*, 2002, 105, 20–25.
- J. Wang, Y. L. Xu, X. Chen, and X. F. Sun, *Compos. Sci. Technol.*, 2007, 67, 2981–2985.
- B. Zhang, Y. Xu, Y. Zheng, L. Dai, M. Zhang, J. Yang, Y. Chen, X. Chen, and J. Zhou, *Nanoscale Res Lett*, 2011, 6, 431–440.
- Y. Yu, C. Ouyang, Y. Gao, Z. Si, W. Chen, Z. Wang, and G. Xue, *J. Polym. Sci. Part A Polym. Chem.*, 2005, 43, 6105–6115.
- X. Zhang, J. Zhang, and Z. Liu, *Appl. Phys. A*, 2005, 80, 1813–1817.
- Y. Zhou, Z.-Y. Qin, L. Li, Y. Zhang, Y.-L. Wei, L.-F. Wang, and M.-F. Zhu, *Electrochim. Acta*, 2010, 55, 3904–3908.
- S. R. Sivakkumar and D.-W. Kim, *J. Electrochem. Soc.*, 2007, 154, A134–A139.
- K. H. An, W. S. Kim, Y. S. Park, J. M. Moon, D. J. Bae, S. C. Lim, Y. S. Lee, and Y. H. Lee, *Adv. Funct. Mater.*, 2001, 11, 387–392.
- K. Jurewicz, S. Delpeux, V. Bertagna, F. Beguin, E. Frackowiak, *J. Power Sources*, 2001, 822, 97–98.
- E. Frackowiak, K. Metenier, V. Bertagna, and F. Beguin, *Appl. Phys. Lett.*, 2000, 77, 2421–2423.
- Y. M. Li, M. van Zijll, S. Chiang, and N. Pan, *J. Power Sources*, 2011, 196, 6003–6006.
- J. Zhang and X. S. Zhao, *J. Phys. Chem. C*, 2012, 116, 5420–5426.
- H. Fu, Z. Du, W. Zou, H. Li, and C. Zhang, *J. Mater. Chem. A*, 2013, 1, 14943–14950.
- US Pat., US2011140658, 2011.
- C. Sasso, E. Zeno, M. Petit-Conil, D. Chaussy, M. N. Belgacem, S. Tapin-Lingua, and D. Beneventi, *Macromol. Mater. Eng.*, 2010, 295, 934–941.
- J. Xu, L. Zhu, Z. Bai, G. Liang, L. Liu, D. Fang, and W. Xu, *Org. Electron.*, 2013, 14, 3331–3338.
- H. Wang, L. Bian, P. Zhou, J. Tang, and W. Tang, *J. Mater. Chem. A*, 2013, 1, 578–584.
- L. M. Huang, T. C. Wen, and A. Gopalan, *Electrochim. Acta*, 2006, 51, 3469–3476.
- D. Müller, C. R. Rambo, D.O.S.Recouvreux, L. M. Porto, and G. M. O. Barra, *Synth. Met.*, 2011, 161, 106–111.
- S. Y. Liew, W. Thielemans, and D. A. Walsh, *J. Phys. Chem. C*, 2010, 114, 17926–17933.
- S. Y. Liew, D. A. Walsh, and W. Thielemans, *RSC Adv.*, 2013, 3, 9158–9162.
- (a) X. Wu, V. L. Chabot, B. K. Kim, A. Yu, R. M. Berry, and K. C. Tam, *Electrochim. Acta*, 2014, 138, 139–147; (b) X. Wu, K.C. Tam, A.P. Yu, R.M. Berry, *Conductive Cellulose Nanocrystals, Method of Producing Same and Uses Thereof*, by, Patent Application No 61/836,319, June 18, 2103
- J. Huang, I. Ichinose, and T. Kunitake, *Chem. Commun.*, 2005, 1717–1719.
- G. Huang, Z., Wang, P. C., MacDiarmid, A. G., Xia, Y., Whitesides, *Langmuir*, 1997, 13, 6480–6484.
- S. F. Lascelles and S. P. Armes, *Adv. Mater.*, 1995, 7, 864–866.
- S. F. Lascelles and S. P. Armes, *J. Mater. Chem.*, 1997, 7, 1339–1347.
- M. J. Burchell and S. P. Armes, *Rapid Commun. Mass Spectrom.*, 2011, 25, 543–550.
- J. Ormond-Prout, D. Dupin, S. P. Armes, N. J. Foster, and M. J. Burchell, *J. Mater. Chem.*, 2009, 19, 1433–1442.
- S. P. Armes, S. Gottesfeld, J. G. Beery, F. Garzon, and S. F. Agnew, *Polymer (Guildf.)*, 1991, 32, 2325–2330.
- J. R. Lovett, L. a. Fielding, S. P. Armes, and R. Buxton, *Adv. Funct. Mater.*, 2014, 24, 1290–1299.
- T. Dai, X. Yang, and Y. Lu, *Mater. Lett.*, 2007, 61, 3142–3145.
- L. Hao, C. Zhu, C. Chen, P. Kang, Y. Hu, W. Fan, and Z. Chen, *Synth. Met.*, 2003, 139, 391–396.
- M. Marini, F. Pilati, and B. Pourabbas, *Macromol. Chem. Phys.*, 2008, 209, 1374–1380.
- R. A. Marcus, *J. Phys. Chem.*, 1963, 67, 853–857.



231x142mm (300 x 300 DPI)